LETTER

doi:10.1038/nature13072

Plate tectonics, damage and inheritance

David Bercovici[1] & Yanick Ricard[2]

The initiation of plate tectonics on Earth is a critical event in our planet's history. The time lag between the first proto-subduction (about 4 billion years ago) and global tectonics (approximately 3 billion years ago) suggests that plates and plate boundaries became widespread over a period of 1 billion years. The reason for this time lag is unknown but fundamental to understanding the origin of plate tectonics. Here we suggest that when sufficient lithospheric damage (which promotes shear localization and long-lived weak zones) combines with transient mantle flow and migrating proto-subduction, it leads to the accumulation of weak plate boundaries and eventually to fully formed tectonic plates driven by subduction alone. We simulate this process using a grain evolution and damage mechanism with a composite rheology (which is compatible with field and laboratory observations of polycrystalline rocks[1,2]), coupled to an idealized model of pressure-driven lithospheric flow in which a low-pressure zone is equivalent to the suction of convective downwellings. In the simplest case, for Earth-like conditions, a few successive rotations of the driving pressure field yield relic damaged weak zones that are inherited by the lithospheric flow to form a nearly perfect plate, with passive spreading and strike-slip margins that persist and localize further, even though flow is driven only by subduction. But for hotter surface conditions, such as those on Venus, accumulation and inheritance of damage is negligible; hence only subduction zones survive and plate tectonics does not spread, which corresponds to observations. After plates have developed, continued changes in driving forces, combined with inherited damage and weak zones, promote increased tectonic complexity, such as oblique subduction, strike-slip boundaries that are subparallel to plate motion, and spalling of minor plates.

The emergence of plate tectonics is arguably Earth's defining moment. How our planet, alone amongst known terrestrial bodies, evolved the unique plate-tectonic form of mantle convection remains enigmatic[3]. Although geochemical and petrological evidence for tectonic activity in Earth's deepest past is difficult to interpret[4], analysis of zircons implies the existence of continental crust and formation of granites more than 4 billion years (4 Gyr) ago[5,6], possibly related to subduction zone melting. Similar evidence suggests that subduction-related crustal production existed 3.6 Gyr ago or earlier[7,8]. However, geochemical and petrologic observations imply that tectonics was not widespread until 3.0–2.7 Gyr ago[9,10]. Whether plate tectonics spread globally over the intervening 1-Gyr interval is of fundamental importance in understanding the emergence of plate tectonics. Moreover, whether the continued accumulation of plate boundaries increased tectonic complexity through geological time remains an open question. Here we propose a plate generation model to argue that transient proto-subduction and accumulated lithospheric damage allowed for the unique emergence and evolution of plate tectonics on Earth.

Plate generation theory generally treats the formation of weak plate boundaries and strong plates by invoking self-weakening feedback mechanisms[3]. Models prescribing steady-state weakening rheologies (for example, viscoplasticity)[11–13] often produce instantaneous plate-like flow, but are not necessarily consistent with rock-deformation experiments, and do not contain the physics to allow dormancy and accumulation of weak zones that become re-activated to form new plate boundaries[14,15]. Damage models of plate generation have, however, been developed to treat self-weakening as well as the evolution of weakness, while also being compatible with laboratory and field observations[1].

Damage mechanics is a continuum theory for how deformation affects material strength, usually by the formation of micro-cracks or reduction of grain size, either of which weakens the material[16]. The pervasiveness of mantle-lithosphere peridotitic mylonites—where localized deformation correlates with reduced mineral grain sizes—at tectonic margins[17,18] indicates that a self-weakening feedback between grain reduction by damage and grain-size-dependent strength (for example, diffusion creep)[19,20] at mid-lithospheric depths is key to plate-boundary formation. This grain-damage feedback mechanism is most plausible and evident in multi-phase or polycrystalline lithospheric rocks (for example, peridotite, which is a mixture of mostly olivine and pyroxene): grain growth in such rocks—which strengthens and heals the material—is known from laboratory and field observations to be impeded by pinning (that is, blocking of grain-boundary migration) by the interface between phases[17,21,22]. Thus, our lithospheric damage mechanism is a coupled evolution model that describes the competition between damage and healing for both grains and interfaces in two-phase assemblages, and where interface pinning both limits grain growth and healing, and promotes damage and shear-localization[1,2] (see Methods for further details).

Our model medium is composed of two components or phases with comparable properties, combined into a 60–40% mixture (as with olivine–pyroxene ratios in peridotite), wherein the grain sizes and the roughness of the interface between phases change according to our evolution model[1,2]. The two-phase grained continuum is incorporated into a horizontal viscous thin-sheet model of convective-type flow in the lithosphere, assuming its strength is dominated by highly viscous flow and mylonitic behaviour at a mid-lithosphere depth (this assumption, however, underestimates weakening and localization at divergent zones due to lithospheric thinning and melting). Flow velocity v is compelled by imposed sublithospheric pressure anomalies P; high or low pressures are akin to mantle convective currents impinging on or separating from this layer. The material rheology is a composite of dislocation creep (that is, viscosity goes inversely as stress squared), which dominates deformation for large grains, and diffusion creep (that is, viscosity goes as grain-size cubed), which dominates for small grains. As deformation and damage drive grain reduction[1], diffusion creep eventually dominates, causing the mixture viscosity $\bar{\mu}$ to reduce where deformation is large, which thus focuses deformation and leads to a self-weakening feedback. If $\bar{\mu}$ were constant, the pressure would drive only divergence or convergence (over positive or negative P, respectively), or sources and sinks of mass in the thin layer, akin to ridges and subduction zones; the divergence rate is denoted by $S=\bar{\nabla}\cdot v$ where $\bar{\nabla}$ is the horizontal two-dimensional gradient operator (see Methods). But with the nonlinear rheology of our medium, horizontal shearing and strike-slip motion can also arise; the vorticity $\Omega=\hat{z}\cdot\nabla\times v$ (where $\hat{z}$ is the vertical unit vector) represents shearing because it measures velocity gradients perpendicular to the flow direction. Moreover, the driving pressure P can also interact with the nonlinear rheology to excite passive divergence that is not directly driven by any pressure anomaly. Focused divergence S and vorticity Ω are important metrics of plate-like flow because

[1]Department of Geology and Geophysics, Yale University, New Haven, Connecticut 06520-8109, USA. [2]Laboratoire de Géologie de Lyon, Université de Lyon 1, CNRS, ENS-Lyon, 69622 Villeurbanne Cedex, France.

they represent convergent, divergent and strike-slip motion on plate boundaries[3]. See Methods for further details.

The model input requires several dimensionless ratios or numbers, which are derived from known physical quantities and laboratory experiments (see Methods). The key parameters controlling the efficiency of plate generation are the damage and healing numbers for both grains and interface; these numbers represent the rates of comminution and coarsening (for either grains or interface), respectively, relative to the rate of deformation. There are three damage numbers, that is, for the interface between phases and the grains of each phase, but they are typically equal to each other, and thus we denote them by one number $\mathcal{D}$; for Earth's conditions, $\mathcal{D}\approx100$. There are likewise three healing numbers, $\mathcal{C}_i$ for grain growth (where $i = 1$ or 2 depending on the phase) and $\mathcal{C}_I$ for interface coarsening; unimpeded grain growth is typically much faster than interface healing[1] and for Earth's conditions we infer that both phases have $\mathcal{C}_i\approx1$, and the interface has $\mathcal{C}_I\approx10^{-5}$. Several tests and comparisons of basic rheological mechanisms are discussed in Methods and shown in Extended Data.

We first consider an idealized model of an early Archaean, single proto-subduction zone or downwelling, by imposing a pressure field P with one focused low-pressure region evolving with time (Fig. 1 top row), which is representative of time-dependent intermittent downwelling inferred to occur in the Archaean[23]. In particular, the first downwelling is akin to a lithospheric drip, which typically cannot readily draw in lithospheric mass, and is therefore ephemeral. A new similar lithospheric downwelling is prescribed to nucleate perpendicularly off a pre-weakened end of the first downwelling, because other orientations would probably be swept away by the initial flow field. The new downwelling is also relatively short-lived, and a third and then fourth downwellings similarly nucleate in turn.

Even with a damage rheology, the first low-pressure region leads only to a convergence zone or sink of lithospheric mass (Fig. 1 left column). During the next downwelling stage, the new flow is influenced by the damaged weak zone left by the original downwelling, whose signature survives because of slow healing; this weak zone becomes a locus of vorticity and strike-slip motion (Fig. 1, second column). In the third stage, the weakness left from the second downwelling is adopted as a strike-slip margin, while that from the original downwelling becomes a focused spreading centre (Fig. 1, third column). As the process is repeated one last time, the accumulated weak zones comprise narrow divergent and strike-slip boundaries, which complement the driving subduction zone to make one contiguous weak plate margin bounding a rapidly moving tectonic plate (Fig. 1, forth column). Moreover, with each subduction zone jump, the divergence field S rebuilds to approximately the same magnitude, but the vorticity Ω progressively grows and finally has a magnitude comparable to that of S (Fig. 1, bottom row). Although the calculation ceases after the last shift in the downwelling, we speculate that the final plate-like flow would organize convection and limit further evolution of cold downwellings and drips by sweeping them into the existing subduction zone.

Although this case is highly idealized, it shows that a fully developed plate can evolve from a downwelling only—where none of the boundaries other than the subduction zone are actively driven—given transience and re-nucleation of the downwelling, and a damage mechanism that provides localization and longevity of weak zones. With these basic ingredients, single proto-subduction zones could build and propagate plate tectonics by accumulating weak zones to be inherited as passive plate boundaries. The time to localize weak zones is several tens of Myr, thus if the time to form new drip downwellings is, with damage[24], a few hundred Myr, then there is sufficient time to develop a full plate in the 1 Gyr between initial proto-subduction and global plate tectonics.

A similar exercise using hotter Venusian surface conditions permits a comparison to Earth's putative twin[25–27]. Using the same material properties but a lithosphere temperature elevated by 200–400 K above the Earth-like case, the damage number $\mathcal{D}$ is reduced by a factor of about 10, and the healing numbers $\mathcal{C}_i$ and $\mathcal{C}_I$ are increased by a factor of up to

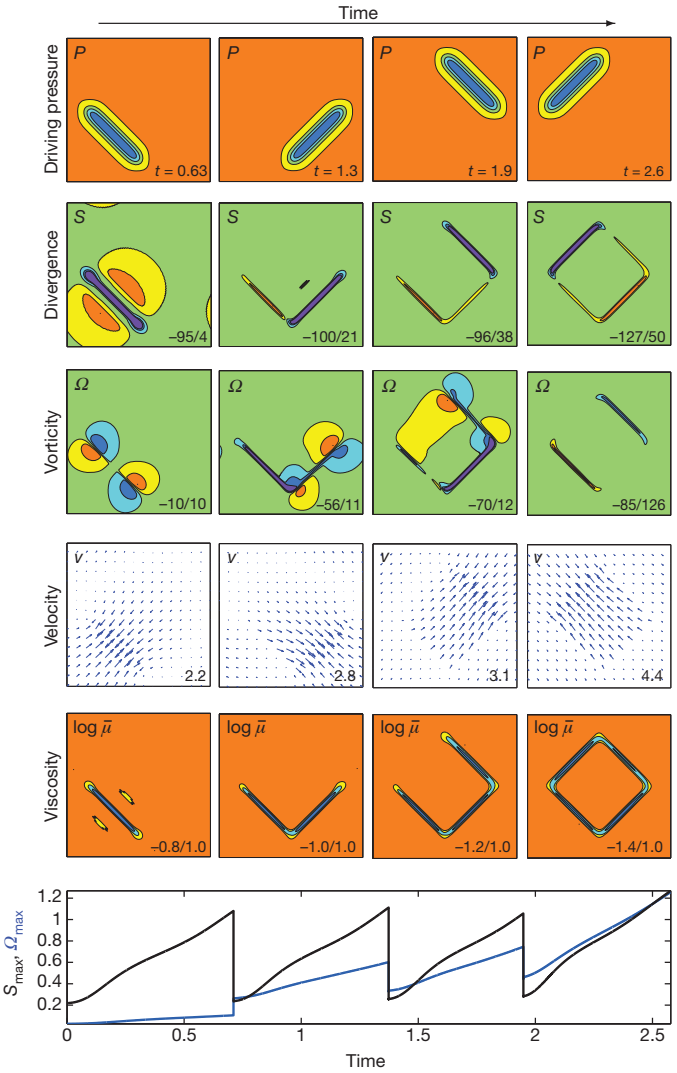

Figure 1 | Lithospheric flow model with damage driven by intermittent proto-subduction. The low in the two-dimensional horizontal pressure field P represents a convective downwelling, rotations of which (top row, with time t indicated) model nucleation of new proto-subduction. Weak regions inherited from previous downwellings localize into passive plate margins, indicated by divergence S, strike-slip vorticity Ω, horizontal velocity v and viscosity $\bar{\mu}$ (rows 2–4). The final state is a four-sided plate, driven by subduction only. Bottom row shows evolution of maximum divergence and vorticity. Scales of distance, time and pressure are ~5,000 km, ~50 Myr and ~300 MPa. Extrema (multiplied by 100, except for log $\bar{\mu}$) are indicated on each frame, save P, which is always 0–1. See Extended Data Fig. 1 for contour details.

10 (see Methods). In this case, as a downwelling migrates to various positions (see Fig. 2), only very faint weak zones accumulate because damage itself is weaker while healing is stronger, thereby resulting in zones of passive divergence and strike-slip vorticity about an order of magnitude weaker than the convergence rate. The final flow field is dominated by convergence, giving the appearance of a subduction-only surface. This result provides a simple explanation for why Venus possibly has subduction zones[28], but no extant plate tectonics.

After the establishment of global plate tectonics and continental growth on Earth, approximately 3 Gyr ago, plate reorganizations became more complicated. Nevertheless, we explore an idealized model of present-day plate motion changes and the resulting accumulation of complexity by inherited weak zones. The experiment is an abstraction of the change in motion of the Pacific plate associated with the 47-Myr-ago Emperor-Hawaiian bend[2,29]. The initial condition has one low-pressure or 'subduction' zone driving a plate-like flow field, similar to the final

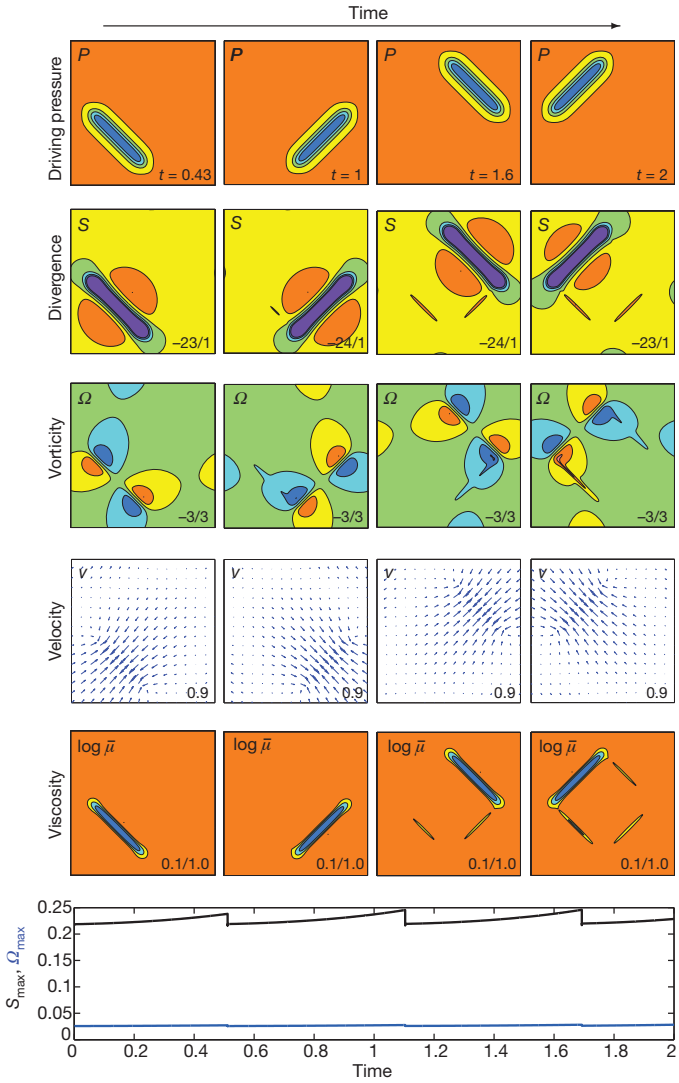

Figure 2 | Lithospheric flow model for Venus. Quantities shown are the same as in Fig. 1 but with parameters appropriate for Venus' higher surface temperature, leading to damage parameter $\mathcal{D}=10$ (instead of 100 for the Earth case) and healing numbers $\mathcal{C}_i=10$ and $\mathcal{C}_I=10^{-4}$ (instead of $\mathcal{C}_i=1$ and $\mathcal{C}_I=10^{-5}$ for the Earth case). Length scale is the same as in Fig. 1, the time and pressure scales are reduced by a factor of about 10 (assuming a 200 K increase in mid-lithosphere temperature from the Earth model[25,27]).

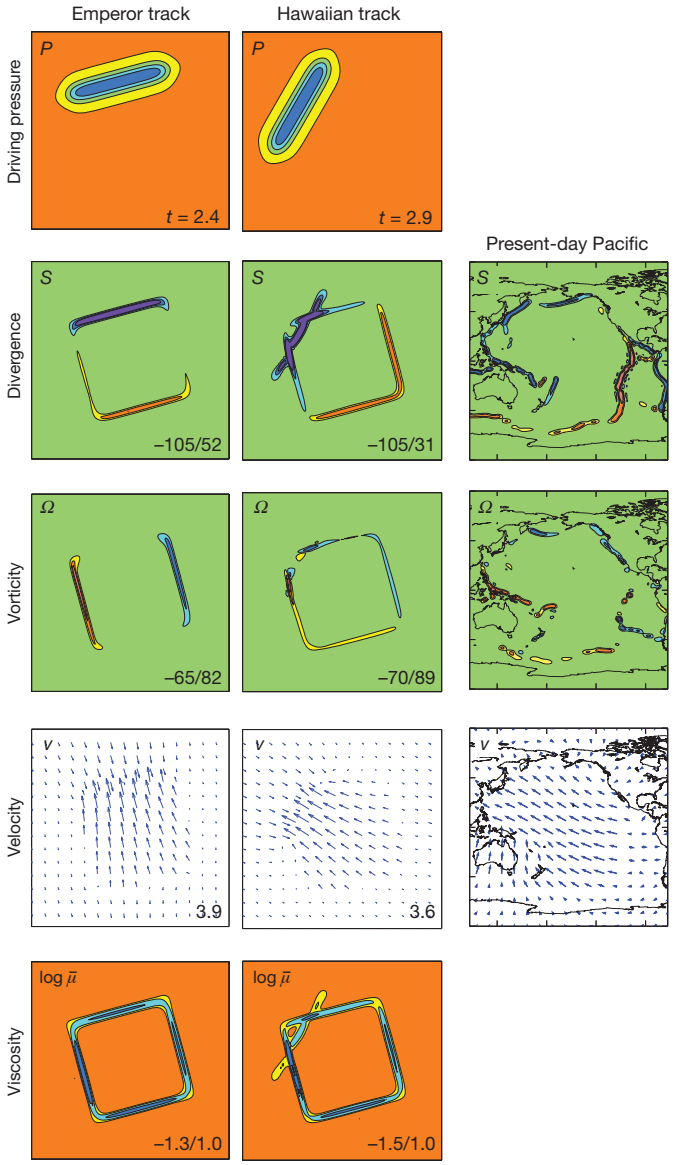

Figure 3 | Lithospheric flow model with Pacific-like rotation. Quantities shown are the same as in Fig. 1 with the same Earth-like parameters. The initial configuration has established plate boundaries, as in the final step of Fig. 1, but in a W15N direction analogous to the Emperor seamount chain trajectory (left column). The pressure field then rotates 45° to W60N analogous to the present-day Hawaiian island chain direction (middle column). Divergence, vorticity and velocity of the Earth's present-day Pacific plate (computed up to spherical harmonic degree 64, using the Nuvel1 plate model[30]) are shown for comparison (right column).

stage shown in Fig. 1. This pressure field initially drives motion north with azimuth 15° west of north (W15N), which is approximately the trajectory of the Emperor seamount chain (Fig. 3 first column). The pressure gradient is then rotated to W60N, roughly the azimuth of the Hawaiian chain (Fig. 3 second column). After the rotation in P, the viscosity $\bar{\mu}$ and thus both the divergence S and vorticity Ω retain 'memory' of the prior plate configuration. Although highly idealized, the experiment yields several features suggestive of present-day Pacific plate motion (Fig. 3 third column). First, the passive divergent zones inherit the older plate geometry and form two ridges wrapping around the southeast corner of the plate, similar to the East Pacific Rise and the Pacific-Antarctic Ridge. The new vorticity field inherits all four of the pre-rotation weak zones, and continues to grow in magnitude; the resulting strike-slip motion is non-orthogonal to the new subduction zone, leading to oblique convergence along the northern boundary, similar to the Aleutian trench, strike-slip motion on the eastern boundary similar to the San Andreas system, and oblique spreading as on the southern Pacific plate. The northern junction between the old and new subduction zones is suggestive of the sharp Aleutian-Kurile arc corner, and the truncated convergent corner of the prior plate is reminiscent of the Philippine plate (see Fig. 3 second column, viscosity field at bottom). In the end, the inheritance of damaged zones by lithospheric flow after a simple change in the slab-pull force leads to several basic features suggestive of Earth's actual Pacific plate.

In summary, we posit that the emergence and evolution of plate tectonics arise by the interaction of a realistic polycrystalline grain-damage mechanism[1,2] and time-dependent subduction, which together allow plate boundary localization and longevity.

METHODS SUMMARY

The theoretical model involves flow in a thin layer of grained, viscous two-phase fluid, wherein the phases represent olivine and pyroxene in a peridotite lithosphere. The layer's rheology is a composite between dislocation and diffusion creep, depending on whether grains are, respectively, bigger or smaller than a critical size. Grain

evolution is coupled to the evolution of the interface between the two phases, which imposes Zener pinning surfaces that block normal grain growth depending on the sharpness of these surfaces. The interface sharpness evolves by the competition between surface-tension-driven coarsening and damage-driven sharpening (that is, distortion, mixing and rending), and sharpened pinning surfaces further block grain growth and facilitate grain-size reduction. When grains shrink enough, they undergo diffusion creep, which depends strongly on grain size, thus leading to a self-softening feedback; that is, deformation reduces grain size and viscosity, which enhances deformation and damage, which reduces grain size and so on. Pinning also prevents healing of small-grained weak zones, depending on temperature; thus weak zones can be inherited and reactivated even after falling dormant. Flow in the thin layer is driven by a low-pressure zone imposed at its base, which represents the pull of a convective downwelling. In a pristine lithosphere, only convergent flow is driven into the low-pressure 'downwelling' and generates a damaged weak zone there. The pressure field is then migrated, and the previously formed, slowly-healing damaged weak zones are inherited by the lithospheric flow and reactivated to form focused divergent or strike-slip zones, or combinations thereof, depending on their alignment. Thus, focused plate boundaries of all types arise by coupling time-dependent downwelling with polycrystalline grain damage. Moreover, as the healing rate of weak zones depends on surface temperature, colder surfaces, as on Earth, promote more intense weak zone formation and inheritance than do much hotter surfaces, as on Venus.

Online Content Any additional Methods, Extended Data display items and Source Data are available in the online version of the paper; references unique to these sections appear only in the online paper.

Received 2 September 2013; accepted 21 January 2014.
Published online 6 April 2014.

1. Bercovici, D. & Ricard, Y. Mechanisms for the generation of plate tectonics by two-phase grain-damage and pinning. *Phys. Earth Planet. Inter.* **202–203,** 27–55 (2012).
2. Bercovici, D. & Ricard, Y. Generation of plate tectonics with two-phase grain-damage and pinning: source–sink model and toroidal flow. *Earth Planet. Sci. Lett.* **365,** 275–288 (2013).
3. Bercovici, D. The generation of plate tectonics from mantle convection. *Earth Planet. Sci. Lett.* **205,** 107–121 (2003).
4. Korenaga, J. Initiation and evolution of plate tectonics on Earth: theories and observations. *Annu. Rev. Earth Planet. Sci.* **41,** 117–151 (2013).
5. Harrison, T. M. *et al.* Heterogeneous Hadean hafnium: evidence of continental crust at 4.4 to 4.5 Ga. *Science* **310,** 1947–1950 (2005).
6. Shirey, S., Kamber, B., Whitehouse, M., Mueller, P. & Basu, A. in *When Did Plate Tectonics Begin on Planet Earth?* (eds Condie, K. & Pease, V.) 1–29 (Special Paper 440, Geological Society of America, 2008).
7. Hopkins, M. D., Harrison, T. M. & Manning, C. E. Constraints on Hadean geodynamics from mineral inclusions in >4Ga zircons. *Earth Planet. Sci. Lett.* **298,** 367–376 (2010).
8. Polat, A., Appel, P. W. & Fryer, B. J. An overview of the geochemistry of Eoarchean to Mesoarchean ultramafic to mafic volcanic rocks, SW Greenland: implications for mantle depletion and petrogenetic processes at subduction zones in the early Earth. *Gondwana Res.* **20,** 255–283 (2011).
9. Condie, K. & Kröner, A. in *When Did Plate Tectonics Begin on Planet Earth?* (eds Condie, K. & Pease, V.) 281–294 (Special Paper 440, Geological Society of America, 2008).
10. Shirey, S. B. & Richardson, S. H. Start of the Wilson cycle at 3 Ga shown by diamonds from subcontinental mantle. *Science* **333,** 434–436 (2011).
11. Trompert, R. & Hansen, U. Mantle convection simulations with rheologies that generate plate-like behaviour. *Nature* **395,** 686–689 (1998).
12. van Heck, H. & Tackley, P. Planforms of self-consistently generated plates in 3D spherical geometry. *Geophys. Res. Lett.* **35,** L19312 (2008).
13. Foley, B. & Becker, T. Generation of plate-like behavior and mantle heterogeneity from a spherical, visco-plastic convection model. *Geochem. Geophys. Geosyst.* **10,** Q08001 (2009).
14. Zhong, S., Gurnis, M. & Moresi, L. Role of faults, nonlinear rheology, and viscosity structure in generating plates from instantaneous mantle flow models. *J. Geophys. Res.* **103,** 15255–15268 (1998).
15. Gurnis, M., Zhong, S. & Toth, J. in *History and Dynamics of Global Plate Motions* (eds Richards, M. A., Gordon, R. & van der Hilst, R.) 73–94 (Geophys. Monogr. Ser. Vol. 121, Am. Geophys. Union, 2000).
16. Krajcinovic, D. *Damage Mechanics* (North-Holland, 1996).
17. Warren, J. M. & Hirth, G. Grain size sensitive deformation mechanisms in naturally deformed peridotites. *Earth Planet. Sci. Lett.* **248,** 438–450 (2006).
18. Skemer, P., Warren, J. M., Kelemen, P. B. & Hirth, G. Microstructural and rheological evolution of a mantle shear zone. *J. Petrol.* **51,** 43–53 (2010).
19. Karato, S., Toriumi, M. & Fujii, T. Dynamic recrystallization of olivine single crystals during high temperature creep. *Geophys. Res. Lett.* **7,** 649–652 (1980).
20. Austin, N. & Evans, B. Paleowattmeters: a scaling relation for dynamically recrystallized grain size. *Geology* **35,** 343–346 (2007).
21. Hiraga, T., Tachibana, C., Ohashi, N. & Sano, S. Grain growth systematics for forsterite ± enstatite aggregates: effect of lithology on grain size in the upper mantle. *Earth Planet. Sci. Lett.* **291,** 10–20 (2010).
22. Linckens, J., Herwegh, M., Müntener, O. & Mercolli, I. Evolution of a polymineralic mantle shear zone and the role of second phases in the localization of deformation. *J. Geophys. Res.* **116,** B06210 (2011).
23. van Hunen, J. & Moyen, J.-F. Archean subduction: fact or fiction? *Annu. Rev. Earth Planet. Sci.* **40,** 195–219 (2012).
24. Paczkowski, K., Bercovici, D., Landuyt, W. & Brandon, M. T. Drip instabilities of continental lithosphere: acceleration and entrainment by damage. *Geophys. J. Int.* **189,** 717–729 (2012).
25. Lenardic, A., Jellinek, M. & Moresi, L.-N. A climate change induced transition in the tectonic style of a terrestrial planet. *Earth Planet. Sci. Lett.* **271,** 34–42 (2008).
26. Landuyt, W. & Bercovici, D. Variations in planetary convection via the effect of climate on damage. *Earth Planet. Sci. Lett.* **277,** 29–37 (2009).
27. Foley, B. J., Bercovici, D. & Landuyt, W. The conditions for plate tectonics on super-earths: inferences from convection models with damage. *Earth Planet. Sci. Lett.* **331–332,** 281–290 (2012).
28. Schubert, G. & Sandwell, D. A global survey of possible subduction sites on Venus. *Icarus* **117,** 173–196 (1995).
29. Sharp, W. D. & Clague, D. A. 50-Ma initiation of Hawaiian-Emperor bend records major change in Pacific plate motion. *Science* **313,** 1281–1284 (2006).
30. Argus, D. F. & Gordon, R. G. No-net-rotation model of current plate velocities incorporating plate motion model NUVEL-1. *Geophys. Res. Lett.* **18,** 2039–2042 (1991).

Acknowledgements D.B. acknowledges support from the National Science Foundation; Y.R. acknowledges support from the Agence Nationale de la Recherche. This work benefitted from discussions with S. Karato, G. Hirth, N. Coltice and B. J. Foley.

Author Contributions D.B. and Y.R. conceived the physical and mathematical model together. D.B. developed and deployed the computational model and was the lead author for the paper.

Author Information Reprints and permissions information is available at www.nature.com/reprints. The authors declare no competing financial interests. Readers are welcome to comment on the online version of the paper. Correspondence and requests for materials should be addressed to D.B. (david.bercovici@yale.edu).

METHODS

Methods Summary. The theoretical model involves flow in a thin layer of grained, viscous two-phase fluid, wherein the phases represent olivine and pyroxene in a peridotite lithosphere. The layer's rheology is a composite between dislocation and diffusion creep, depending on whether grains are, respectively, bigger or smaller than a critical grain size. Grain evolution is coupled to the evolution of the interface between the two phases, which imposes Zener pinning surfaces that block normal grain growth depending on the sharpness of these surfaces. The interface sharpness evolves by the competition between surface-tension-driven coarsening and damage-driven sharpening (that is, distortion, mixing and rending), and sharpened pinning surfaces further block grain growth and facilitate grain-size reduction. When grains shrink enough, they undergo diffusion creep, which depends strongly on grain size, thus leading to a self-softening feedback; that is, deformation reduces grain-size and viscosity, which enhances deformation and damage, which reduces grain-size, and so on. Pinning also prevents healing of small-grained weak zones, depending on temperature; thus weak zones can be inherited and reactivated even after falling dormant. Flow in the thin layer is driven by a low-pressure zone imposed at its base, which represents the pull of a convective downwelling. In a pristine lithosphere, only convergent flow is driven into the low pressure 'downwelling' and generates a damaged weak zone there. The pressure field is then migrated, and the previously formed, slowly-healing damaged weak zones are inherited and reactivated to form focused divergent or strike-slip zones, or combinations thereof, depending on their alignment. Thus, focused plate boundaries of all types arise by coupling time-dependent downwelling with polycrystalline grain damage. Moreover, since the healing rate of weak zones depends on surface temperature, colder surfaces, as on Earth, promote greater weak zone formation and inheritance than much hotter surfaces, as on Venus.

Damage theory and flow model details. Following Bercovici and Ricard[1,2], our model continuum has two phases of comparable density, viscosity and other properties, combined into a non-dilute mixture. The phase volume fractions ϕ_i are assumed uniform and constant (where $i = 1$ or 2 denotes the primary or secondary phase, that is, $\phi_1 = 40\%$ for pyroxene and $\phi_2 = 60\%$ for olivine in mantle-lithosphere peridotite). The phases each have unique grain-size distributions with mean grain-sizes $\mathcal{R}_i$, which evolve separately. The interface separating the phases is described by a scalar interface density α, which represents the interfacial area per unit volume of the mixture[31], and is associated with an interface radius of curvature, or interface 'roughness' r. Zener pinning[32,33] occurs if a grain, of either phase, is growing and the migration of its boundary is obstructed by the interface with the other phase; the interface density α represents the concentration of obstructing boundaries and the interface roughness r controls the effectiveness of the resulting pinning.

The flow field kinematics are described in Bercovici and Ricard[2], wherein, because the silicate phases in the mixture are highly viscous and tightly coupled, they have the same velocity field v. The mixture itself is incompressible, and thus $\nabla\cdot v = 0$, which is guaranteed by the relation

$$v = \nabla\times(\psi\hat{z}) + \nabla\times\nabla\times(\theta z\hat{z}) \tag{1}$$

where ψ is the toroidal stream function and θ is the poloidal potential, and, in the thin-sheet model both are functions of x, y and time t only. The horizontal divergence of the velocity

$$S = \bar{\nabla}\cdot v = \nabla^2\theta \tag{2}$$

represents a source-sink field associated with divergent and convergent zones. Focused strike-slip toroidal motion is represented by concentrated bands of vertical vorticity

$$\Omega = \hat{z}\cdot\nabla\times v = -\nabla^2\psi \tag{3}$$

Our thin-sheet flow model deviates from that of Bercovici and Ricard[2] since it involves imposition of a driving pressure field; it thus solves for both S and Ω (rather than imposing S) from the conservation of momentum in creeping two-phase flow with grained phases[1]

$$0 = -\nabla\bar{\Pi} + \nabla\cdot\bar{\tau} + \bar{\rho}g \tag{4}$$

where the pressure Π, stress τ and density ρ are volume averaged over the two phases (that is, for any quantity q, $\bar{q} = \sum_i \phi_i q_i$); g is gravitational acceleration; and Π_i includes the effect of surface tension on the interface between phases and on the grain boundaries[1,34]. The volume averaged stress tensor is

$$\bar{\tau} = \bar{\mu}\left(\nabla v + [\nabla v]^{\mathrm{t}}\right) \tag{5}$$

where $\bar{\mu}$ is the volume average of the viscosities μ_i, the rheological model of which is discussed below. The lateral driving force for the system is a pressure gradient acting on the lithosphere from the underlying mantle. In particular, we impose a pressure field in the mantle P due to, for example, buoyant upwellings and heavy downwellings. Continuity of normal stress across the boundary between the lithospheric layer and the mantle requires

$$-\bar{\Pi} + 2\bar{\mu}\frac{\partial w}{\partial z}\bigg|_l = -P + 2\mu_m\frac{\partial w}{\partial z}\bigg|_m \tag{6}$$

where w is vertical velocity and $|_j$ indicates evaluation on the lithospheric ($j = l$) or mantle ($j = m$) side of the boundary. On the lithospheric side $\partial w/\partial z = -S$. On the mantle side we assume that the material passing across the boundary reaches a negligible absolute velocity at some greater depth d in the mantle; thus, the mantle stress imparts resistance to flow being injected into or ejected out of the lithosphere. At the base of the lithospheric layer, $w \approx Sh$, where h is the lithospheric thickness, (that is, $\partial w/\partial z \approx -w/h \approx -S$) then in the mantle $\partial w/\partial z \approx Sh/d$, in which case we write the lithospheric pressure $\bar{\Pi}$ in terms of the driving mantle pressure P as

$$\bar{\Pi} = P - 2\left(\bar{\mu} + \breve{\mu}\right)S \tag{7}$$

where $\breve{\mu} = \mu_m h/d$. In this way pressure anomalies from the mantle are transmitted to the lithosphere but with some reduction caused by resistance to exchanging mass between the lithosphere and mantle. If we assume for example that the major resistance to the downwelling is support of a cold slab impinging on the 660 km boundary, then μ_m is comparable to the cold-lithospheric viscosity and $h/d \approx 1/5$. Since there is some resistance by drag on the side of the slab as well, we use $\breve{\mu} \approx 3\boldsymbol{\mu}/8$ for the calculations shown, where $\boldsymbol{\mu}$ is the reference lithosphere viscosity (used for non-dimensionalizing the equations, as discussed below); solutions are not sensitive to the exact value of $\breve{\mu}$ provided it is a modest fraction of $\boldsymbol{\mu}$. Substituting (5) and (7) into (4) and taking $\bar{\nabla}\cdot$ of the resulting equation leads to an elliptic equation for the divergence S

$$\begin{aligned}\left(3\bar{\mu} + 2\breve{\mu}\right)\nabla^2 S &= \nabla^2 P - 7\nabla\bar{\mu}\cdot\nabla S + 2\hat{z}\cdot\nabla\bar{\mu}\times\nabla\Omega \\ &-2\left(S\nabla^2\bar{\mu} + \Delta^*\bar{\mu}\frac{\partial^2\psi}{\partial x\partial y} - \frac{\partial^2\bar{\mu}}{\partial x\partial y}\Delta^*\psi + \nabla\nabla\bar{\mu} : \nabla\nabla\theta\right)\end{aligned} \tag{8}$$

where we define the differential operator $\Delta^* = \partial^2/\partial x^2 - \partial^2/\partial y^2$ (ref. 35). Similarly, taking $\hat{z}\cdot\nabla\times$ of (4) with (5) results in an elliptic equation for the vorticity Ω

$$\begin{aligned}\bar{\mu}\nabla^2\Omega &= -2\nabla\bar{\mu}\cdot\nabla\Omega - \hat{z}\cdot\nabla\bar{\mu}\times\nabla S \\ &+\Delta^*\bar{\mu}\left(\Delta^*\psi - 2\frac{\partial^2\theta}{\partial x\partial y}\right) + 2\frac{\partial^2\bar{\mu}}{\partial x\partial y}\left(\Delta^*\theta + 2\frac{\partial^2\psi}{\partial x\partial y}\right)\end{aligned} \tag{9}$$

The rheological model reflects a mixture or composite of dislocation and diffusion creep mechanisms[1,2,36], which leads to the viscosity relation

$$\mu_i = \frac{1}{2}\left(a_i\tau_i^{n-1} + \frac{b_i}{\mathcal{R}_i^m}\right)^{-1} \tag{10}$$

where $\tau_i^2 = \frac{1}{2}\tau_i:\tau_i$ is the second stress invariant for phase i (and given equation (5), $\tau_i = \mu\bar{\tau}/\bar{\mu}$). a_i and b_i are, respectively, the dislocation and diffusion creep compliances for phase i, n is the power-law index (typically $n = 3$), and m is the grain-size exponent (typically either 2 for Nabarro-Herring or 3 for Coble creep); the exponents n and m are assumed the same for both phases for simplicity. The composite rheology (10) implies that the transition from dislocation to diffusion dominated creep occurs for the macroscopic parcel at a critical grain size $\mathcal{R}_c = \left[b_i/\left(a_i\tau_i^{n-1}\right)\right]^{1/m}$; thus, a parcel whose mean grain size is far from this critical value is predominantly undergoing one creep mechanism or the other.

The evolution of the mean grain size $\mathcal{R}_i$ is coupled to the evolution of the interface roughness r; these evolution laws follow from non-equilibrium thermodynamics[1] and lead to

$$\frac{D\mathcal{R}_i}{Dt} = \frac{G_i}{p\mathcal{R}_i^{p-1}}\mathcal{Z}_i - \lambda\frac{\mathcal{R}_i^2}{3\gamma_i}f_{\mathrm{G}}(1-f_{\mathrm{I}})\Psi_i\mathcal{Z}_i^{-1} \tag{11}$$

$$\frac{Dr}{Dt} = \frac{\eta G_{\mathrm{I}}}{qr^{q-1}} - \frac{r^2}{\eta\gamma_{\mathrm{I}}}f_{\mathrm{I}}\bar{\Psi} \tag{12}$$

where G_i and G_{I} are coarsening coefficients for the grain boundaries and interface, respectively, p and q are exponents (typically $p = 2$ and $q \approx 4$), γ_i and γ_{I} are the surface energies on grain boundaries and interface between phases respectively. and $\eta \approx 3\phi_1\phi_2$. The deformational work in phase i is $\Psi_i = \tau_i^2/\mu_i$; f_{I} is a constant partitioning fraction governing how much deformational work goes towards creating

interface surface energy, while the remaining fraction going towards creating grain-boundary energy[1,2,36]

$$f_G = f_G^* \left(1 + \left(\frac{\mathcal{R}_c}{\mathcal{R}_i}\right)^m\right)^{-1} \quad (13)$$

is prescribed, by dynamic recrystallization theory, to only be significant for material undergoing dislocation creep, that is, when $\mathcal{R}_i > \mathcal{R}_c$, and where f_G^* is the maximum possible value of f_G. The interface blocking of grain growth is given by the Zener pinning factor

$$\mathcal{Z}_i = 1 - c(1-\phi_i)\frac{\mathcal{R}_i^2}{r^2} \quad (14)$$

where $\lambda = 4.95$ and $c = 0.87$ for the grain-size distribution used by Bercovici and Ricard[1,2]. The Zener pinning effect acts to slow down and even reverse grain growth as r becomes comparable to or smaller than $\sqrt{c(1-\phi_i)}\mathcal{R}_i$, and facilitates damage to grains. However, given the recrystallization limitation (13), damage is more effective at distorting and sharpening the interface, which then forces grain-size reduction by pinning (through the factor $\mathcal{Z}_i$), driving the medium into diffusion creep. In this way damage and self-weakening in the diffusion creep regime coexist, which is nominally disallowed in single-phase minerals.

The dimensionless governing equations are derived using the amplitude of the driving pressure field $\max|P| = \mathbf{P}$ as the basic stress scale controlling the dynamics of the system; in this case, the rate scale for S, Ω and inverse of time is $\mathbf{S} = \bar{a}\mathbf{P}^n$, where $\bar{a} = \sum_i \phi_i a_i$, and the macroscopic length scale is $\mathbf{L}$, the characteristic separation of the high and low pressure zones, or equivalently the length of the low-pressure zone if that is all that is specified. The viscosity and grain-size scales are $\boldsymbol{\mu} = \mathbf{P}/\mathbf{S} = \mathbf{P}^{1-n}/\bar{a}$ and $\mathbf{R} = \left(\bar{b}\boldsymbol{\mu}\right)^{1/m}$ where $\bar{b} = \sum_i \phi_i b_i$. We thus non-dimensionalize time according to $t = \mathbf{S}^{-1}t'$, spatial variables according to $(x,y,z) = \mathbf{L}(x',y',z')$, $\nabla = \mathbf{L}^{-1}\nabla'$, and the dependent variables according to $(S,\Omega,v,\theta,\psi) = \mathbf{S}(S',\Omega',\mathbf{L}v', \mathbf{L}^2\theta', \mathbf{L}^2\psi')$, $\left(P, \underline{\tau}_i\right) = \mathbf{P}\left(P', \underline{\tau}'_i\right)$, $\mu_i = \boldsymbol{\mu}\mu'_i$ and $(\mathcal{R}_i, r) = \mathbf{R}\left(\mathcal{R}'_i, r'\right)$. With these scaling relationships, the dimensionless governing equations for flow are, after dropping the primes, unchanged from (1)–(3), (8) and (9). The dimensionless relation for rheology is the same as (10), except for replacing a_i with $\boldsymbol{a}_i = a_i/\bar{a}$, and b_i with $\mathbf{b}_i = b_i/\bar{b}$. In general we expect comparable rheologies between the two phases such that $a_1 \approx a_2$ and $b_1 \approx b_2$ in which case we can assume $\mathbf{a}_i \approx \mathbf{b}_i \approx 1$. The dimensionless evolution equations for $\mathcal{R}_i$ and r become[2]

$$\frac{D\mathcal{R}_i^p}{Dt} = \mathcal{C}_i\mathcal{Z}_i - \frac{1}{2}\mathcal{D}_i\mathcal{R}_i^{p+1}\mathbf{a}_i\tau_i^{n+1}\mathcal{Z}_i^{-1} \quad (15)$$

$$\frac{Dr^q}{Dt} = \mathcal{C}_I - \frac{1}{4}\mathcal{D}_I r^{q+1}\bar{\tau}^2/\bar{\mu} \quad (16)$$

where

$$\mathcal{C}_i = \frac{G_i}{\mathbf{S}\mathbf{R}^p} \quad , \quad \mathcal{C}_I = \frac{\eta G_I}{\mathbf{S}\mathbf{R}^q} \quad (17)$$

and

$$\mathcal{D}_i = \frac{4p\lambda f_G^*(1-f_I)\mathbf{R}\mathbf{S}^{1/n}}{3\gamma_i\bar{a}^{1/n}} \quad , \quad \mathcal{D}_I = \frac{4qf_I\mathbf{R}\mathbf{S}^{1/n}}{\eta\gamma_I\bar{a}^{1/n}} \quad (18)$$

are the coarsening and damage numbers for grains and interface, respectively, and the relation for the Zener pinning factor $\mathcal{Z}_i$ does not change from (14).

The dimensionless parameters are inferred using a typical tectonic stress scale of $\mathbf{P} \approx 300$ MPa and otherwise follow the development outlined by Bercovici and Ricard[2]; the authors there used experimental numbers for rheology and grain-growth summarized by Rozel *et al.*[36], except for a higher grain-growth activation energy typical of ionic diffusion in olivine[37] of ~300 kJ mol^{-1} as opposed to the 200 kJ mol^{-1} quoted from Karato[38], which is for lower pressures and also considered unusually low[39,40]. We thus use $p = 2$ and $q = 4$ for which we obtain[2] $\mathcal{C}_i \approx 1$, $\mathcal{C}_I \approx 10^{-5}$, and $\mathcal{D}_i = \mathcal{D}_I = 100$ (hence we refer to only one damage number $\mathcal{D}$ in the main text). For cases relevant to Venus we reduce the tectonic stress scale by ~10 and increase the mid-lithosphere temperature by 200 K (refs 25, 26), which leads to increasing $\mathcal{C}_i$ and $\mathcal{C}_I$ by as much as ~10 and decreasing $\mathcal{D}_i$ and $\mathcal{D}_I$ by ~10. The implicit non-dimensionalizing length and time scales are discussed in Figs 1 and 2. We keep the power-law index fixed at $n = 3$ for simple dislocation creep, and $m = 3$ for Coble creep in the main text. However, below we also compare results between cases with various rheologies, from constant viscosity to the full grain-damage and pinning model with composite rheology. Numerical solutions of the nonlinear governing equations are found using the same method described by Bercovici and Ricard[2], with the additional flow equation (8) solved the same way as other nonlinear elliptic equations, for example, (9). The sensitivity of solutions to key parameters, especially the damage number $\mathcal{D} = \mathcal{D}_I = \mathcal{D}_i$, are discussed in Bercovici and Ricard[2].

Model tests and comparison of rheological mechanisms. Stationary flow in an initially pristine lithosphere: we compare the characteristics of plate generation for several rheological mechanisms, with a symmetric pressure field P that has both high and low pressure zones. We step through levels of complexity going from Newtonian ($b_i = 0$, $n = 1$), to pure steady-state dislocation creep power law rheology ($b_i = 0$ and $n = 3$), to grain-damage without Zener pinning ($m = n = 3$ but fixing $\mathcal{Z}_i = 1$), and finally to the general case of grain-damage with Zener pinning ($m = n = 3$ and $\mathcal{Z}_i$ variable). Comparison of these mechanisms (see Extended Data Fig. 1) demonstrates their efficacy in plate generation. A uniform Newtonian rheology is known to prohibit the generation of toroidal motion and provides the standard of non-plate-like motion; in this case the divergence field S is a mirror image of the pressure P, and the velocity traces dipolar potential flow field lines, as expected. Pure dislocation creep causes slight sharpening of the divergence field and generates finite but weak toroidal motion; the resulting velocity field differs little from the Newtonian case. When grain-damage occurs without Zener pinning, there is only grain reduction while the two phases deform via dislocation creep, that is, at high stress and large grain size. This case is equivalent to the single-phase system[36] since there is no influence of one phase on the other through pinning. In the pressure-driven model, damage without pinning provides only modest focusing of S and more toroidal motion, which is modestly better than the pure dislocation creep case[1,2]. In the case with both damage and Zener pinning, the divergence field S is much more focused and intense than in previous cases, and toroidal vorticity Ω is more focused and band-like and the velocity field distinctly more plate-like. However, in these cases the divergence and convergent zones differ in magnitude, with the maximum convergence rate being approximately double the divergence rate. The vorticity Ω is also not as focused as S, and its magnitude is usually comparable to the divergence rate but half the convergence rate.

Orthogonal rotations and plate-boundary inheritance: the toroidal motion generated from a pristine lithosphere yields significant plate-like motion, yet is still modest relative to generated poloidal motion. As discussed in the main text, additional focusing of strike-slip zones is assisted by inheriting previous weak zones. Here we test how various rheologies generate weak zones that can be inherited to develop focused plate boundaries. As a simpler version of experiments performed in the main text, we first drive flow as above (Extended Data Fig. 1) and after the divergence and vorticity fields are well established, we rotate the driving pressure P by 90° (see Extended Data Fig. 2). Thus, if established weak zones before the rotation have memory (that is, do not vanish), they can be inherited by the new toroidal field. Performing this experiment with basic dislocation creep shows that, as expected, there are no inherited weak zones and the vorticity field is exactly the same, and as weak, as before the rotation. The experiment using grain damage without pinning, leads to moderate inheritance of weak zones; however, while the peak strike-slip vorticity increases after the rotation, it plateaus and never reaches the same magnitude as the divergence field, and grain size stops reducing on reaching the diffusion-dislocation creep boundary thus limiting the extent of self-softening and localization (Extended Data Fig. 2, bottom left). The experiment with damage and pinning yields highly localized and intense strike-slip vorticity Ω whose maximum values even exceed the maximum divergence and convergence rates, and the minimum grain-size continues to drop even while in diffusion creep (Extended Data Fig. 2, bottom right).

31. Bercovici, D., Ricard, Y. & Schubert, G. A two-phase model of compaction and damage, 1. general theory. *J. Geophys. Res.* **106,** 8887–8906 (2001).
32. Smith, C. S. Grains, phases, and interfaces: an interpretation of microstructure. *Trans. AIME* **175,** 15–51 (1948).
33. Hillert, M. Inhibition of grain growth by second-phase particles. *Acta Metall.* **36,** 3177–3181 (1988).
34. Ricard, Y. & Bercovici, D. A continuum theory of grain size evolution and damage. *J. Geophys. Res.* **114,** B01204 (2009).
35. Bercovici, D. A simple model of plate generation from mantle flow. *Geophys. J. Int.* **114,** 635–650 (1993).
36. Rozel, A., Ricard, Y. & Bercovici, D. A thermodynamically self-consistent damage equation for grain size evolution during dynamic recrystallization. *Geophys. J. Int.* **184,** 719–728 (2011).
37. Karato, S. *Deformation of Earth Materials: An Introduction to the Rheology of Solid Earth* (Cambridge Univ. Press, 2008).
38. Karato, S. Grain growth kinetics in olivine aggregates. *Tectonophysics* **168,** 255–273 (1989).
39. Evans, B., Renner, J. & Hirth, G. A few remarks on the kinetics of static grain growth in rocks. *Int. J. Earth Sciences. Geol. Rundsch.* **90,** 88–103 (2001).
40. Faul, U. H. & Scott, D. Grain growth in partially molten olivine aggregates. *Contrib. Mineral. Petrol.* **151,** 101–111 (2006).

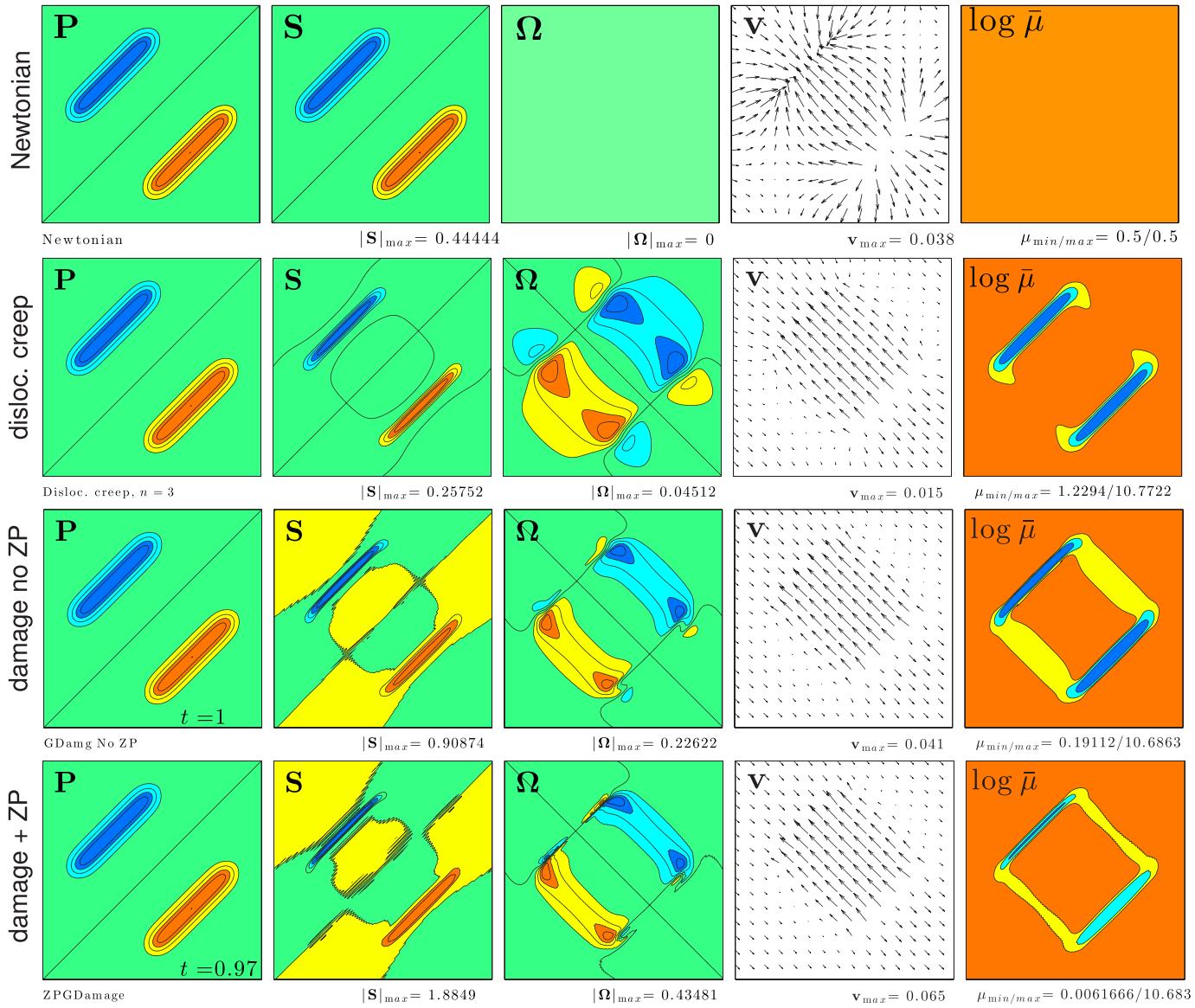

Extended Data Figure 1 | Horizontal two-dimensional lithospheric flow calculations impose a driving force (that is, high and low pressures akin to ridge push and slab pull) *P*, to generate a poloidal divergent/convergent 'source-sink' field *S*, toroidal strike-slip vorticity *Ω*, and horizontal velocity field *v*. For a Newtonian lithospheric fluid (first row), *S* simply mirrors the pressure *P*, there is no vorticity and the velocity field follows dipolar field lines and is very un-plate-like. For a basic non-Newtonian dislocation-creep power-law (strain-rate $\propto$ stress^n, where $n = 3$; see second row), divergence is slightly altered, a weak vorticity field is generated and the velocity is still largely dipolar. Using the full two-phase grain damage with and without Zener pinning[1] (ZP; third and fourth rows), *S* is sharpened considerably, a significant *Ω* field is generated, and the velocity is more plate-like; however, the approach to plate-like behaviour is more profound with Zener pinning. Contours are evenly spaced between extrema, except for *S* and *Ω*, which are between $\pm$min(max(*Q*), |min(*Q*)|), where $Q = S$ or *Ω*, and saturate at indigo (for negative values) or light red (positive values). The extremal values are indicated below each frame (except for *P* which is always between -1 and 1).

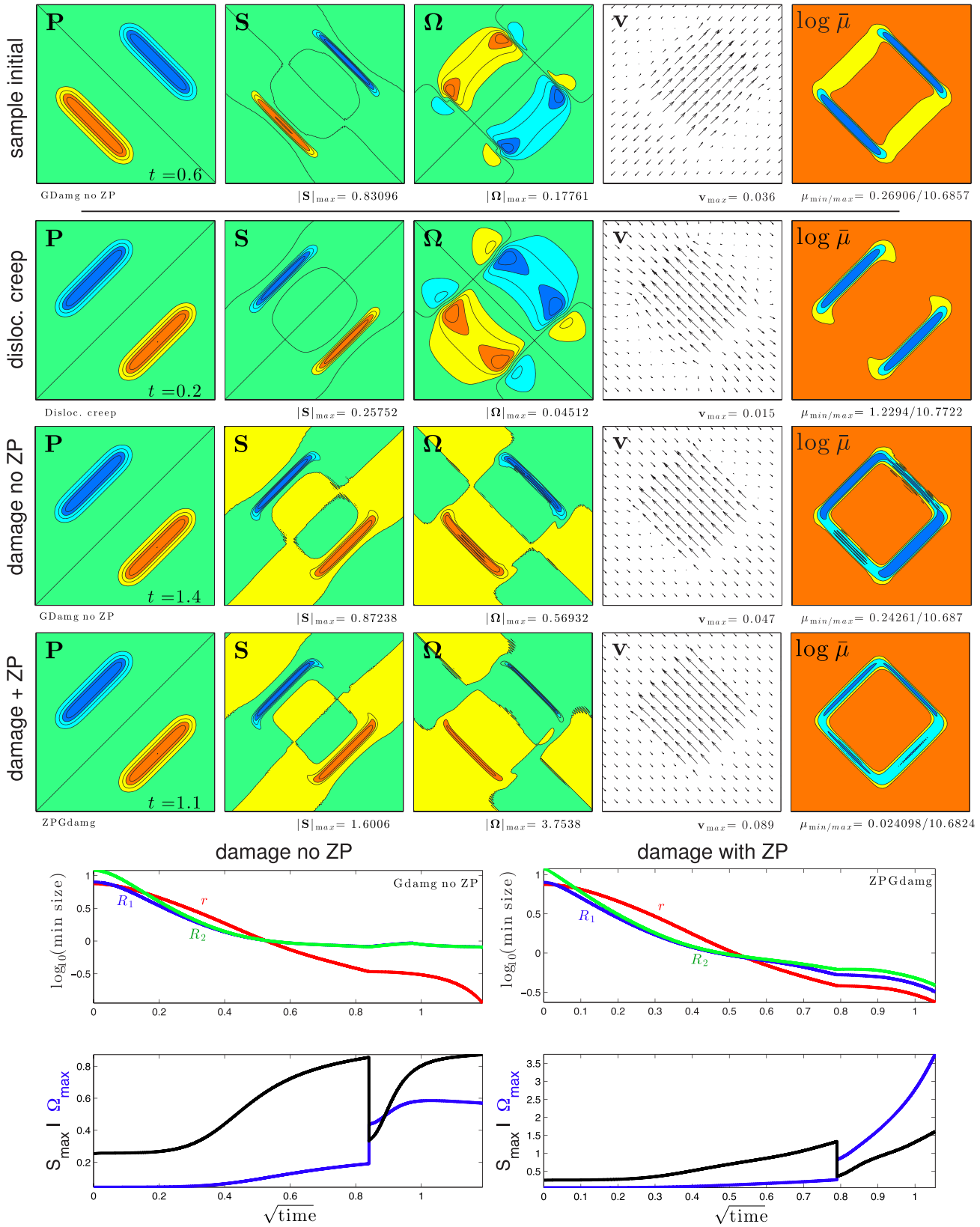

Extended Data Figure 2 | Case where the driving pressure field *P* rotates by 90° and the vorticity field *Ω* inherits the weak zone of the prior divergence field. The topmost row shows a sample initial condition before rotation (in particular for the case with grain-damage but no Zener pinning). The subsequent three rows are for simple dislocation creep, grain damage without pinning, and grain damage with pinning. The bottom-most frames show the time evolution for minimum grain sizes $\mathcal{R}_i$ of each phase (green for the primary 'olivine' phase, blue for the secondary 'pyroxene' one), interface roughness r, and maximum divergence S and vorticity Ω, for the grain-damage cases with and without Zener pinning. See also Extended Data Fig. 1 for a description of contoured variables.